KSCE Journal of Civil Engineering (2014) 18(6):1641-1649

DOI 10.1007/s12205-014-0490-6

Geotechnical Engineering

pISSN 1226-7988, eISSN 1976-3808
www.springer.com/12205

Study on the Hydromechanical Behavior of Single Fracture under Normal Stresses

Ni Xie*, Jinbao Yang, and Jianfu Shao*****

Received September 27, 2012/Revised March 11, 2013/Accepted October 11, 2013/Published Online June 20, 2014

Abstract

The coupling between hydraulic and mechanical behavior of the fractured rock mass is of great significance for various civil and environmental engineering projects. In order to study the hydro-mechanical behavior of single fracture, seepage tests under different confining pressures and fracture water pressures were conducted on single shear fractures produced by triaxial loading of diabase rock samples from Danjiangkou Water Reservoir, China. Test results show that fluid pressure acting on fracture surfaces has strong influences on the hydraulic behavior of the fracture. Based on the classic Biot poroelasticity theory and by taking the fracture as assembling of a set of voids in rock mass, a generalized Biot coefficient is introduced to describe the interaction effect between pore fluid pressure and fracture deformation. Then, a nonlinear constitutive equation for single fracture under both normal stress and fluid pressure is developed. Later, the mechanical deformation of the fracture is related to the fracture hydraulic conductivity through "cubic law", so that a coupled mechanical-hydraulic model is proposed. All the four parameters involved in this model have their physical significances and can be determined through mechanical compression tests and seepage tests. A first validity of the model is made by predicting the variation of fracture flowrates versus normal stress under different fluid pressures.

Keywords: *hydromechanical behavior, single rock fracture, seepage tests, generalized biot coefficient*

1. Introduction

The coupling between hydraulic and mechanical behavior of the fractured rock mass is of great significance in civil and environmental engineering projects. Especially for the Reservoir Induced Seismicity (RIS), various research results show that the distribution and magnitude of pore pressure have direct relevance to the occurrence of RIE (Lee-Bell and Nur, 1978; Gupta, 2001 & 2002; Do Nascimento, 2005). Augment in pore pressure can either reduce the effective normal stresses in faults or lower down the stability level of the basing rockmass of the reservoir, thus leading to the generation of RIE of various magnitudes. For the fractured rockmasses, the accurate simulation of pore pressure field needs to take into consideration the coupled interaction between solid phase (mechanics) and fluid phase (hydraulics), or we can call it hydromechanical behavior as an integral definition. Obviously, the hydromechanical behavior of fractured rock masses is dominated by that of single fractures, since the permeability of rock matrix (intact rock) is fairly low compared to the hydraulic conductivity of single fracture. As a result, stress-flow coupling of single fracture, which is fundamental to hydromechanical analysis of fractured rock mass, becomes one of the emphasized issues in rock mechanical research, and the research achievements can be applied to natural gas/oil exploitation, underground radioactive waste repositories, seepage flow through tunnels and underground caverns, reservoir-induced earthquakes, etc.

The opening of a fracture, which is the most important parameter in determining the hydraulic conductivity of the fracture, is directly relevant to the stress condition it exposed to (Chang *et al*., 2004; Zhang and Wang, 2006; Zhou *et al*., 2008). Therefore, a great amount of work has been done to obtain the transmissivity characteristics of single fracture under different stress conditions. Many of these studies investigated the validity of theoretical flow laws derived from the classical "cubic law" (Snow, 1968), which was derived from smooth parallel plate model, and employed a corrective factor adjusting the relation between the mechanical and hydraulic aperture based on the experimental results or numerical simulations (For instance, Witherspoon *et al.*, 1980; Barton, 1982; Esaki *et al.*, 1999; Barton and Olsson, 2001; Liu *et al*., 2003; He and Yang, 2004; Davy *et al*., 2007; Zhang and Wang, 2006; Zhou *et al.*, 2008). For the experimental studies, most of the previous researchers produced single fractures through Brazilian splitting test (Davy *et al*., 2007), or by bonding two intact rocks together to form a single fracture

*Lecturer, Faculty of Engineering, China University of Geosciences, Wuhan, 430074, China (Corresponding Author, E-mail: shelly93111@163.com)
**Engineer, Three Gorges Geotechnical Consultants Co., LTD., Wuhan 430074, China (E-mail: dabaowuda@163.com)
***Professor, Laboratory of Mechanics of Lille, University of Lille I, Cite Scientifique, 59655 Villeneuve d'Ascq, France (E-mail: Jian-Fu.Shao@polytech-lille.fr)

(He and Yang, 2004). However, for the latter method, the asperity and waviness of the natural fractures cannot be well simulated. While for the former one, the interlocking of the artificial fractures is obviously looser than that of the natural ones due to the debris lost along fracture surfaces.

While for the theoretical modeling of the hydromechanical behavior of fractures, preliminary researches usually focus on the effects of stresses on fracture deformation and its hydraulic conductivity, from normal to shear stresses and combined stress states. Various types of models can be found in literatures for the description of fracture deformation, from simple nonlinear elastic models to elasoplastic ones and damage mechanics (For instance, Goodman, 1976; Tsang and Witherspoon, 1981, 1983; Barton *et al.*, 1985; Barton and de Quadros, 1997; Olsson and Barton, 2001; Shao *et al*., 2005; Koyama *et al*., 2009). In all these models, however, only the effects of external stresses are well investigated, and the part of deformation caused by inner fluid pressure is not taken into account. But in engineering practices the effect of fluid pressure on fracture deformation should not be ignored, especially when the pore pressure is relatively great compared to the external stresses. In fact, fracture deformation and the variation of fluid pressure within it are coupled with each other inherently. The fluid pressure can cause deformation in fracture, meanwhile, fluid pressure varies as fracture deforms. For instance, when fracture aperture gets smaller, fluid will be expelled from the space between the two fracture faces, leading to a decrease in the "effective" fluid pressure acting on fracture surface. As the fracture is narrowed to completely closing, fluid pressure levels off to zero. Thus, to well describe the hydromechanical behavior of single fracture, the interaction between fluid pressure and fracture deformation should be properly investigated.

Therefore, in this chapter, we try to study the hydromechanical behavior of the freshly produced shear fractures under different stress conditions. Diabase rock samples were firstly loaded to shear failure to obtain a shear fracture, and then in-situ seepage tests under different confining pressures and fracture water pressures were carried out to study the transmissivity characteristics of the shear fracture. The test results show that most of the rock samples produce a single running-through shear fracture, which allows us to study the test results with the model of single fracture within a rock mass. The experimental observations also show that besides the applied normal stresses, the fluid pressure acting on fracture surfaces also has strong influence on the hydraulic behavior of the fracture. Based on the experimental data, a couple poromechanical model of single fracture subject to normal stresses is proposed based on the generalized Biot poroelastic theory, with particular emphasis given to the influence of fluid pressure on fracture deformation, as will be shown in the following sections.

2. Experimental Apparatus and Procedure

2.1 Experimental Apparatus

Diabase rock was chosen as the testing material because it is one of the most widely distributed rocks in the area of Danjiangkou Water Reservoir located in Hubei Province, Central China, which is the water source of the 'South-to-north water diversion' project. The diabase rock samples were cored from a slightly weathered rock taken from the surface layer of Danjiangkou Water Reservoir, with a intensity of 2.91 g/cm^3, void ratio of 2.69% and the uniaxial compressive strength of 102.9 MPa. All the samples were deaired by a vacuum pump for 4 hours and then immerged in distilled water for more than 48 hours to get saturated, making sure that the seepage within the samples is single phase flow.

The triaxial rheometer developed and manufactured in France is adopted as the testing device in this experiment, because it can apply axial load, confining pressure and pore pressure independently and can be used to do water seepage test at the same time. The dimension of rock sample is ϕ50×100 mm, and there are two Linear Variable Displacement Transducers (LVDT) fixed to both left and right sides of the sample to measure the axial strain, and an electronic strain transducer fixed on a steel ring with a nick to measure the lateral strain. The steel ring has the same inner diameter as the rock sample and is placed exactly at the mid-height of the sample. The stress and strain data can be automatically collected by the attached computer. A photo of the testing system is shown in Fig. 1.

Fig. 1. Exterior Appearance of the Experimental Instrument

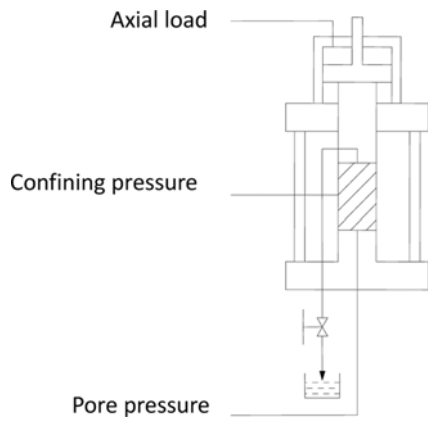

Fig. 2. Sketch of the Triaxial Cell

Pore pressure within the sample in the form of water pressure is infiltrated from the bottom of the sample and discharged from the top, as can be seen from Fig. 2. It is also the driving pressure differential and the source of seepage water during the seepage tests. When the valve connecting to the top is open, pore pressure on top of the sample becomes zero and a one-dimensional seepage flow generates under the pressure gradient between upper and lower surface of the sample.

2.2 Experimental Procedures

The rock samples, subjected to a net confining pressure of 2 MPa firstly, were then axially loaded to shear failure by means of displacement loading with a loading rate of 0.05 mm/min. After the samples were loaded to shear failure, the axial deviatoric pressure was then unloaded to zero and the isotropic compression stress state was kept. During the whole process, the pore pressure was also applied to the samples with the water yielding valve kept open. All 11 rock samples that we tested by the loading procedure mentioned above generated one single shear fracture, which enables us not only to use the transmissivity theory of single fractures conveniently, but also to obtain single natural fractures under triaxial stress condition as a better alternative to Brazilian splitting test, because this method will not cause rock debris lose at fracture surfaces.

If the sample generated a shear fracture running from the upper surface to the lower surface as is shown in Fig. 3, there would be water running out of the outlet, then the measurement of flowrate started. However, if the fracture started from the upper surface of the sample but ended above the lower surface, which meant there was no running-through channel for seepage water to reach the outlet on top of the sample, then it would be impossible to obtain the flowrate of the fracture. In this case, the sample was taken as failed. Among all the 11 samples that we tested, only 2 of them failed to generate a running-through shear fracture.

Seepage tests under different confining pressures and fluid pressures were then conducted on rock samples with single running-through shear fracture. We carried out 3 sets of tests in total, with the fluid pressure of 1 MPa, 3 MPa and 5 MPa for each set of samples respectively. During the process of seepage tests, the diabase sample was subjected to hydrostatic compressive loading. Thus the fracture was subjected to normal stress only, denoted by σ_n, the magnitude of which is identical to that of the hydrostatic confining pressure. The pore pressure imposed at the bottom of the sample (at the other end of the sample, the pore pressure is zero) is taken as the injection fluid pressure p for the evaluation of the net confining pressure as $\sigma_{net} = \sigma_n - p$, which increases by steps of 2 MPa, 5 MPa, 10 MPa, 15 MPa and 20 MPa. At each step, the flow rate was recorded after the stabilization of both fluid flow and the axial and lateral strains.

3. Experimental Results and Analysis

3.1 Flowrate and Confining Pressure

Figure 4 shows the variation of flowrate Q versus confining pressure σ_n up to a net confining pressure of 20 MPa for 3 samples under 3 different injection fluid pressures, which also indicates 3 different pressure gradients within the fractures. It can be seen from the curves that with the increment of net confining pressure, the flowrate of the fracture decreases dramatically, especially in the anterior phase when the net confining pressure is no more than 10 MPa. After that, fracture flowrate decreases much more smoothly and levels off to a constant value in the end.

It is also shown in Fig. 4 that under the same net confining pressure, the fracture flowrate increases with the augment of injection fluid pressure, and this increment seems to be more significant when the confining pressure is relatively small. The augment in flowrate indicates an increment in the fracture hydraulic aperture. With regard to fractured rock mass, biggish fluid pressure will cause additional deformation in the bilateral rock matrixes of the fracture. Especially when the net confining pressure is just a little greater than the inner fluid pressure, this kind of additional deformation becomes even more obvious, which results in increment in fracture aperture and hydraulic conductivity. To conclude, the increment of transmissivity of a fracture is primarily related to the fracture aperture, and both confining pressure and fluid pressure have influences on it.

Fig. 3. Diabase Rock Samples after Shear Failure with Single Running-through Fracture

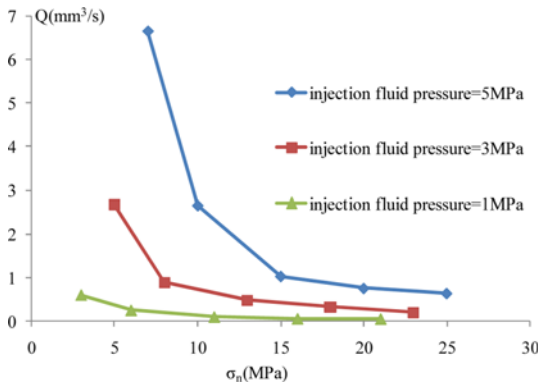

Fig. 4. Variation of Volumetric Flowrate with Confining Pressure

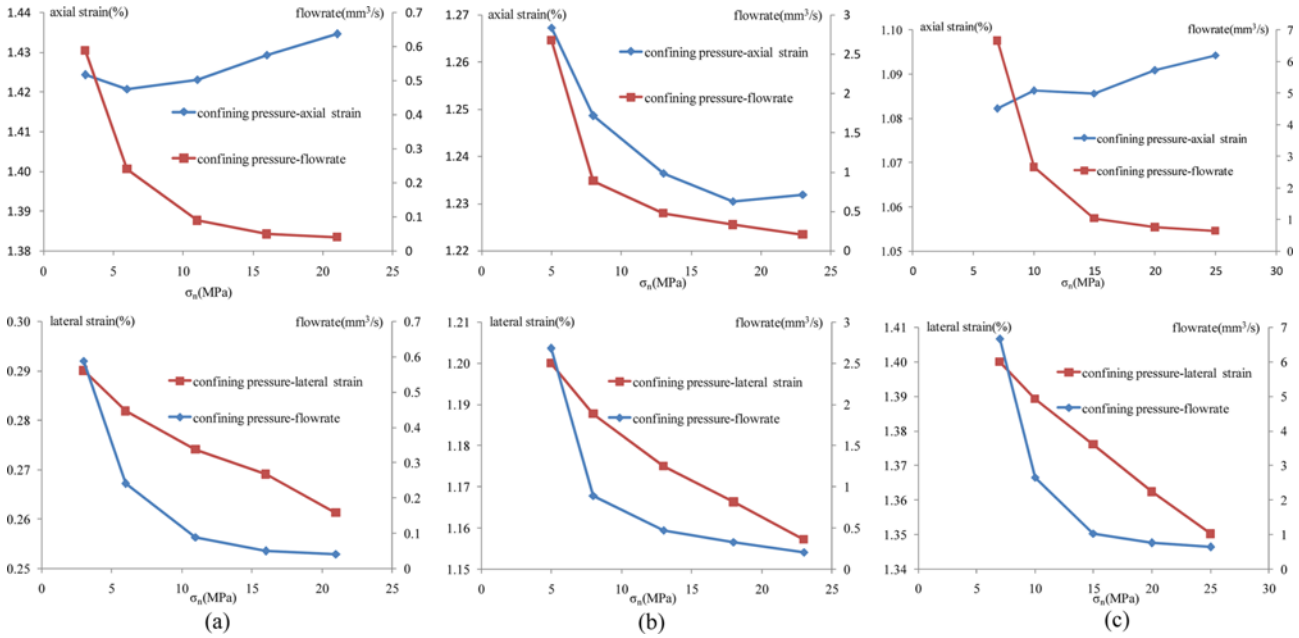

Fig. 5. Flowrate and Both Axial and Lateral Strain Responses of Different Rock Samples: (a) No.02 Sample with Injection Fluid Pressure of 1 MPa, (b) No.47 Sample with Injection Fluid Pressure of 3 MPa, (c) No.32 Sample with Injection Fluid Pressure of 5 MPa

3.2 Flowrate and Strains

Both axial and lateral strains were collected automatically by the attached computer during seepage test. The stabilized strains after each loading of confining pressure were selected and plotted in Fig. 5, where the axial strain (ε_1) takes downward compression as positive, and the lateral strain (ε_3) takes circumferential compression as negative.

It is shown in Fig. 5 that during seepage test, the axial strains of the rock samples vary little with the increment of confining pressures with a variation range between ±3%. Meanwhile there seems to be no unified variation pattern, since the No.32 and No.02 samples get compressed while the No.47 sample gets rebounded as the confining pressure increases. Thus, link between axial strain and fracture transmissivity is not so explicit.

On the contrary, the lateral strains of all samples show an approximately linear decrement with the increment of confining pressure, indicating the rock samples are circumferentially compressed. This transverse compression is related to flowrate variation through its influence on fracture aperture. Since the elastic modulus of rock matrix is much more rigid than that of the fracture, a large portion of the lateral strain will be attributed to the deformation of the fracture aperture. Therefore the change of lateral strain can indicate the variation of fracture aperture and correspondingly the fracture transmissivity to a certain degree.

It can be seen from Fig. 5 that the lateral strains decrease approximate linearly with the increase of the confining pressure, indicating that the rock samples are circumferentially compressed at an even rate. However the decreasing rate of flowrate is not even but reduces gradually. After the confining pressure reaches certain values (e.g. for No. 02 sample it is nearly 10 MPa), the reduction of fracture flowrate becomes much smaller and nearly keeps constant, while the lateral strain still increases.

This phenomenon can be explained as follows: As the confining pressure increases in the earlier phase, the fracture is compressed easily and the fracture aperture becomes smaller, which leads to a dramatic decrement in permeability of the fracture. Meanwhile there are more areas between fracture surfaces getting into contact due to fracture compression. When the confining pressure continues to increase afterwards, these contact areas are able to withstand significant stresses while maintaining space for fluids to continue to flow, even that the fracture aperture continues to decrease. Similar conclusions can be found in Witherspoon *et al*. (1980). In fact, the mechanical response to the augment in contact area of the fracture surface is reflected by the increase in fracture stiffness. Hence, the influence of confining pressure on fracture permeability is actually substantiated through its effect on fracture stiffness.

Besides, from the lateral strain values of the 3 rock samples in Fig. 5, it can be seen that the larger the fracture water pressure is, the greater the lateral strain values will be, which indicates again that the additional deformation of the rock matrix caused by fracture water pressure can't be ignored.

4. Formulation of the Hydromechanical Model

4.1 Modeling of Fracture Deformation under Fluid Pressure

In geomechanics studies, when inner fluid pressure is taken into consideration, the simplest method is to combine it with the external stresses linearly as $\sigma' = \sigma - p$ (p denotes for fluid pressure and take compression as positive), which we call the Terzaghi effective stress. However, the experimental observations

by various researchers (Barton and Olsson, 2001; Haji-Sotoudeh, 1995) as well as ourselves show that the deformation of fracture due to increment in fluid pressure is different from that due to increment in external stresses, thus the utilization of Terzaghi effective stress can't describe the effect of fluid pressure on fracture deformation properly.

Inspired by previous work of Tsang and Witherspoon (1981), we assume that the fracture within rockmass is assembling of a set of connected voids saturated by fluid under local conditions, and fracture deformation is a result of the closure or opening of these voids. Based on this hypothesis, we can extend the classical Biot poroelasticity theory to the modeling of rock fractures, or in other words, we implement the Biot effective stress to describe the effect of fluid pressure on fracture deformation. By introducing the relative normal displacement ε_n as the ration between total normal displacement Δu_n and initial fracture aperture b_i, i.e. $\varepsilon_n = \Delta u_n / b_i$, the constitutive equations for the saturated fracture can be obtained based on the Biot poroelastisity theory as (Bart *et al.*, 2004):

$$d\sigma_n = K_n(\varepsilon_n)d\varepsilon_n + B(\varepsilon_n)dp \tag{1}$$

where Δu_n is the normal displacement of the fracture and takes compression as positive (the same as σ_n); b_i is the initial fracture aperture when the applied stresses is null, and also corresponds to the maximum normal displacement when the normal compressive stress approaches infinite; B denotes the generalized Biot coefficient; K_n in Eq. (1) stands for the normal stiffness of the fracture and is expressed in MPa. It should be noted that K_n is a function of fracture displacement, since fracture stiffness will get increased as the fracture aperture decreases mainly due to the augment in contacting area between fracture faces. Meanwhile, fluid flow through fracture also depends on the connectivity of voids and the ratio of uncontacted areas. Therefore fracture stiffness and fluid flow within it are related to each other implicitly (see details in Pyrak-Nolte and Morris, 2000).

4.2 Physical Significance of K_n and Its Empirical Expression

A lot of empirical expressions of K_n have been proposed by researchers based on the experimental data of fracture compression tests. The typical ones include the hyperbolic law proposed by Bandis and Barton (Bandis *et al*., 1983; Barton *et al.*, 1985) and the classic exponential function, etc. Here in this work, we propose the following expression to describe the relationship between normal stiffness K_n and displacement increment of the fracture based on the experimental data in Haji-Sotoudeh (1995) where the displacement-stress curves of a granite fracture in loading-unloading cycles are presented

$$u_n = b_i\left|1 - \frac{1}{\ln\left(\frac{\sigma_n}{K_n}+1\right)+1}\right| \tag{2}$$

in which K_{ni} (in MPa) denotes the initial normal stiffness of the fracture when applied normal stress is zero. Eq. (2) satisfies the following limit conditions: when $\sigma_n = 0$, $u_n = 0$; and when $\sigma_n \to \infty$, $u_n \to b_i$. As a visual presentation, Fig. 6 gives the displacement-stress curve described by Eq. (2) and the experimental data obtained from loading-unloading normal compression tests of a granite fracture respectively. For the calculated curve, parameter values are chosen as: $K_{ni} = 0.8$ MPa, $b_i = 123.5$ μm. Comparison between the test and computational data in 6 shows that Eq. (2) can well describe the nonlinearity pattern of the fracture displacement under normal stress.

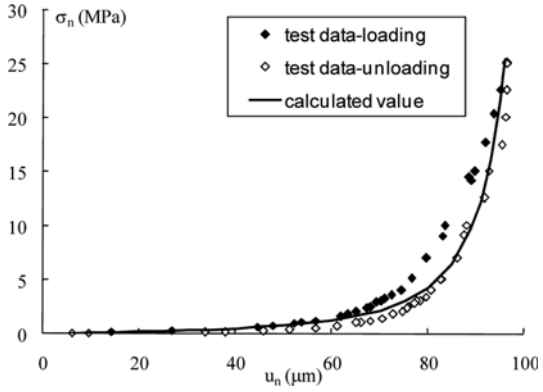

Fig. 6. Normal Stress - Displacement Diagram of a Granite Fracture: Comparison between Experimental Data (after Haji-Sotoudeh, 1995) and the Calculation Results by Eq. (2)

From Eq. (2) we can get the relationship between normal stress σ_n and relative displacement of the fracture $\varepsilon_n (= u_n / b_i)$ as:

$$\sigma_n = K_{ni}\left[\exp\left(\frac{\varepsilon_n}{1-\varepsilon_n}\right) - 1\right] \tag{3}$$

Derivation of Eq. (3) with respect to ε_n gives the expression of normal stiffness K_n as:

$$K_n = \frac{d\sigma_n}{d\varepsilon_n} = \frac{K_{ni}}{(1-\varepsilon_n)^2}\exp\left(\frac{\varepsilon_n}{1-\varepsilon_n}\right) \tag{4}$$

or equivalently as:

$$K_n = \frac{K_{ni}}{(1-u_n/b_i)^2}\exp\left(\frac{u_n}{b_i - u_n}\right) \tag{5}$$

We can see from Eq. (5) that when $u_n = 0$, it turns out that $K_n = K_{ni}$. Thus, Eq. (5) guarantees the physical meaning of K_n at the same time.

4.3 Physical Significance of B and Its Expression

In the theoretical framework of Biot poroelasticity for porous media, the coupling effect between fluid pressure and pore deformation is reflected through the Biot coefficient. As in the present model pertinent to rock fracture, the generalized Biot coefficient B takes the same role as the traditional one.

In accordance with the classic poromechanics, we first consider a specific loading path, which is to let the fluid pressure within fracture and the external normal stress increase simultaneously, i.e. we set $d\sigma_n = -dp$. With the help of Eq. (1) we can get the relative displacement of the fracture corresponding to this specific loading path as:

$$d\varepsilon_n = \frac{-[1+B(\varepsilon_n)]dp}{K_n(\varepsilon_n)} \tag{6}$$

Similar to poromechanics, this loading path can be taken as compression of the solid frame of rock matrix. Therefore, the normal displacement of the fracture can also be expressed as follows:

$$d\varepsilon_n = \frac{-dp}{K_s} = \frac{d\sigma_n}{K_s} \tag{7}$$

where K_s is the elastic modulus of the rock solid matrix in the normal direction of the fracture. The stress-stain curves under this loading of $d\sigma_n = -dp$ can be obtained by "unjacketed tests", and K_s is just the slope of that curve.

Comparison between Eqs. (6) and (7) leads to the expression of the generalized Biot coefficient B as:

$$B(\varepsilon_n) = 1 - \frac{K_n(\varepsilon_n)}{K_n} \tag{8}$$

Equation (8) shows that the Biot coefficient B is related to both the normal stiffness of the fracture and the elastic modulus of the solid frame of rock matrix. Since normal stiffness K_n is a function of fracture displacement ε_n, the Biot coefficient B is correspondingly also a function of ε_n. As the compressive displacement of the fracture ε_n increases, normal stiffness K_n increases too, leading to a decrease of the Biot coefficient B. Both K_n and B are relevant to the current displacement condition of the fracture.

With regard to the densely compacted rocks with very low porosity, we can approximately take the macro bulk modulus of the rock as identical to that of the solid frame in rock matrix, i.e. $K_s = K_r$. In this way, we can get the value of K_s through conventional triaxial compression tests.

4.4 Modeling of Fluid Flow Through Single Fracture

At sufficiently low flow rates, the cubic law developed for incompressible fluid flowing in smooth parallel plates is applied to describe fluid flow along a fracture (Snow, 1968, 1969).

$$Q = \frac{\Delta p_f}{12\mu H} e_h^3 \tag{9}$$

where Q is the volumetric flow rate through a fracture per unit time (expressed in m^3/s), μ is the dynamic viscosity of the fluid (expressed in Pa·s), Δp_f denotes the fluid pressure difference between the two ends of the fracture, H stands for the length of the fracture along the direction of fluid flow, and e_h represents the hydraulic aperture of the fracture.

Due to the asperity of fracture surfaces, the hydraulic aperture e_h is not identical to the mechanical aperture of the fracture but is related to it by an empirical relationship proposed by Barton *et al.* (1985) as:

$$e_h = \frac{(b_i - u_n)^2}{\mathrm{JRC}^{2.5}} \tag{10}$$

where JRC denotes the joint roughness coefficient, and both e_h and b_i are expressed in micron (μm).

The fracture displacement u_n in Eq. (10) is obtained by constitutive Eq. (1), thus the combination of Eqs. (1), (9) and (10) establishes the modeling of fluid flowrate through a single fracture with special pertinence on the coupling between flowrate and fluid pressure. The fracture displacement caused by fluid pressure is realized through the Biot coefficient; in return, Biot coefficient is a function of the fracture displacement at the same time. They interact with each other in a coupled way.

5. Application to Seepage Tests

The hydromechanical model of single fracture proposed above is now applied to the seepage tests that we conducted as a first validation. The first step in model application consists in the determination of the four parameters.

5.1 Determination of the Mechanical Parameters K_{ni} and b_i

In the seepage tests that we conducted, hydrostatic compression stress state is kept after the generation of the single fracture. Thus the fracture is subjected to normal stress only during seepage test, the magnitude of which is identical to that of the hydrostatic compression stress. Moreover, the external confining stress gets increased step by step whereas the fluid pressure keeps unchanged during the seepage test. Therefore the stress increment on fracture is just the augment in compression stress.

Assume that the intact rock is much more rigid than the fracture so that the total strain of the sample is completely attributed by the deformation of the fracture, we can then get the fracture normal displacement u_n through a conversion of the axial or lateral displacement of the sample as: $\Delta u_n = \frac{\Delta u_1}{\sin\beta} = \frac{\Delta u_3}{\cos\beta}$ with Δu_1 and Δu_3 standing for the axial and lateral displacement increment of the sample respectively (both of them can be deduced from Fig. 5), and b denoting the angle between the fracture plan and vertical direction, as shown in Fig. 7.

Based on the experimental data of normal displacements versus normal stresses of the fracture, we can get the values of

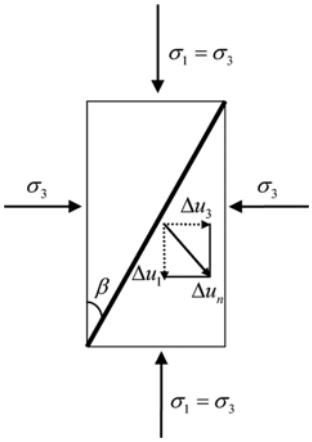

Fig. 7. Schematic Diagram of the Rock Sample with a Single Running-through Fracture under Triaxial Loading

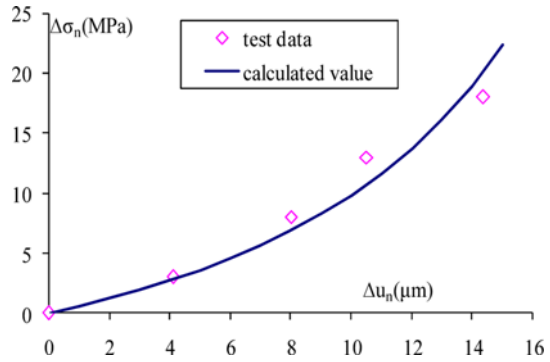

Fig. 8. Fitting of Parameters K_{ni} and b_i from Fracture Normal Stress-displacement Testing Results using Eq. (3)

K_{ni} and b_i through data fitting by utilizing Eq. (3). A comparison between the test data and fitting curve of No. 02 fracture (with a fluid pressure of 1 MPa) is shown in Fig. 8 where the fitting data are K_{ni} = 20 MPa and b_i = 35 μm. Analogously, the values of K_{ni} and b_i for fracture No. 47 (with a fluid pressure of 3 MPa) and No. 32 (with a fluid pressure of 5 MPa) can also be obtained by the same method.

5.2 Determination of b_i Through Seepage Test

As a matter of fact, since the mechanical aperture is directly related to the hydraulic one, the initial mechanical aperture b_i can also be determined by the results of seepage test as an alternative to the mechanical tests which we have just introduced in the previous section.

If we take the intact rock as totally impermeable and all the seepage fluid flows through the fracture, we can get the hydraulic apertures under different loading levels through Eq. (9). Thus, the experimental data of fracture displacement versus hydraulic aperture can be obtained during the seepage test, based on which b_i and JRC can be determined through optimal fitting using Eq. (10).

A comparison between the displacement-hydraulic aperture test data and fitting curve of No. 02 fracture (with a fluid pressure of 1 MPa) is shown in 9 where the fitting results are b_i = 35 μm and JRC = 12. The same approach is applied to No. 32 and No. 47 fractures and the final values of the parameters that

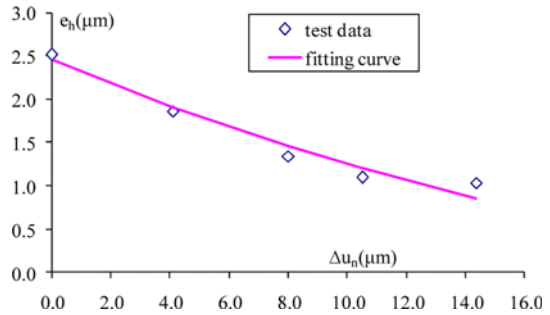

Fig. 9 Fitting of Parameters b_i and JRC from Fracture Normal Displacement-hydraulic Aperture Testing Results using Eq. (10)

Table 1. Obtained Values of Parameters K_{ni}, b_i and JRC for Three Fractures

Sample	K_{ni} (MPa)	b_i (μm)	JRC
No. 02 (fluid pressure = 1 MPa)	20	35.5	12.0
No. 47 (fluid pressure = 3 MPa)	18	50.5	15.0
No. 32 (fluid pressure = 5 MPa)	19	54.0	15.0

have been chosen for the numerical modeling of the three samples are listed in Table 1.

We can see from that the difference in JRC of the three fractures is not significant, mainly due to the fact that the generation conditions of the three fractures are almost the same. Meanwhile,

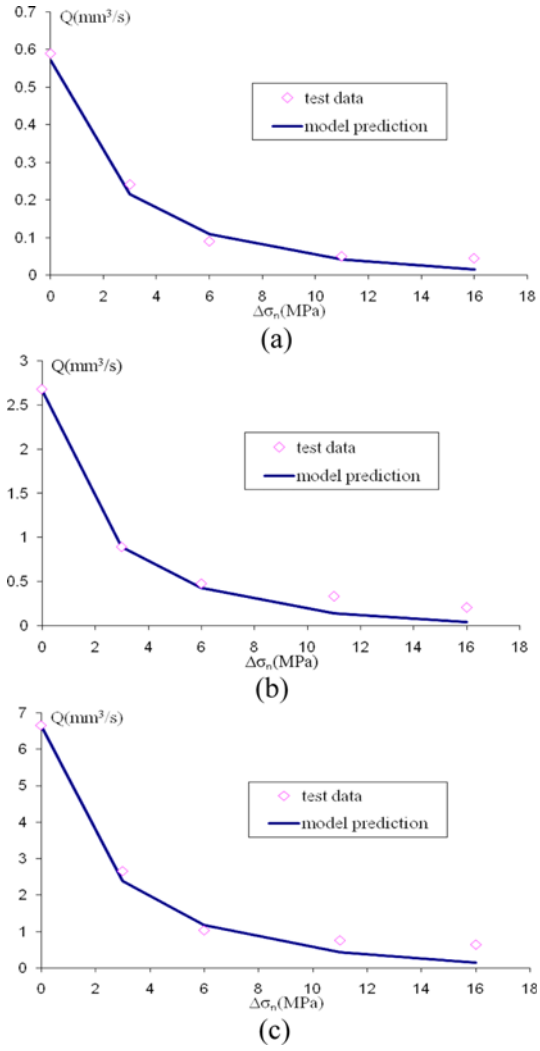

Fig. 10. Fluid Flowrate versus Normal Stress of Three Fractures under Three Different Fluid Pressures: Comparison between Test Data and Model Predictions: (a) No.02 Fracture (Fluid Pressure p = 1 MPa), (b) No. 47 Fracture (Fluid Pressure p = 3 MPa), (c) No. 32 Fracture (Fluid Pressure p = 5 MPa)

the fracture subjected to larger fluid pressure has a greater initial aperture b_i, indicating the fluid pressure within fracture is beneficial to the expansion of fracture aperture. Moreover, the initial stiffness K_{ni} of the fracture having a large initial aperture b_i will be relatively small, which further substantiates the rationality of the fitting results.

5.3 Preliminary Validation of the Model in Seepage Test

By employing parameters listed in Table 1, the flowrates of the three fractures during the process of normal pressure loading are predicted and the results are compared with the experimental data, as shown in Fig. 10. A good agreement can be found between the test data and model predictions, demonstrating that the proposed model can well describe the variation of flowrate with the change of normal stress. Still it should be noted that during the seepage tests we conducted, the fluid pressure is kept invariant. Thus only the effect of normal stress variation on fracture deformation and seepage flow is reflected. More testing data are needed for further validation of the model.

6. Conclusions

The diabase rock samples from Danjiangkou Water Reservoir were firstly deviatorically loaded to shear failure to obtain a single fracture, and then seepage tests under different confining pressures and fluid pressures were carried out to study the hydromechanical behavior of the fracture. Experimental results show that generally the flowrate through the newly-generated fracture decreases with the increase of confining pressure, but with different decrease rates at different loading phases. The fluid pressure also has obvious influences on flowrate mainly due to the phenomenon that fluid pressure can induce an additional deformation in the rock matrix which causes an increment in fracture aperture and correspondingly the hydraulic conductivity. Therefore, it is strongly recommended to consider the effects of both external loads and fluid pressure on the deformation and seepage of rock mass respectively.

Based on the experimental observations, formulation for the hydromechanical modeling of single fracture was established with the special pertinence to the effect of fluid pressure on fracture deforamtion. By taking the fracture as a collection of connected voids in rock mass, a generalized Biot coefficient, which is not a constant but a function of fracture deformation, is introduced to describe the interaction effect between pore fluid pressure and fracture deformation, so that the dependency of the effect of fluid pressure on fracture deformation is emphasized. With the help of the generalized Biot coefficient, a nonlinear constitutive equation for a single fracture under both normal stress and fluid pressure is developed based on the Biot poroelasticity theory. Later, the mechanical deformation of the fracture is related to the fracture hydraulic conductivity through "cubic law", so that a coupled mechanical-hydraulic model is developed. Comparison between model prediction and tests data verifies the applicability of the proposed model. All the above work can provide theoretical references for the calculation of pore pressure in reservoir area and contribute to mechanism study of reservoir induced seismicity.

References

Bandis, S. C., Lumsden, A. C., and Barton, N. R. (1983). "Fundamentals of rock joint deformation." *International Journal of Rock Mechanics and Mining Sciences and Geomechanics Abstracts*, Vol. 20, No. 6, pp. 249-268.

Bart, M., Shao, J. F., Lydzba, D., and Haji-Sotoudeh, M. (2004). "Coupled hydromechanical modeling of rock fractures under normal stress." *Canadian Geotechnical Journal*, Vol. 41, No. 4, pp. 686-697.

Barton, N. (1982). *Modelling rock joint behaviour from in situ block tests: Implications for nuclear waste repository design*, Office of Nuclear Waste Isolation, Columbus, OH, ONWI-308.

Barton, N., Bandis, S. C., and Bakhtar, K. (1985). "Strength, deformation and conductivity coupling of rock joints." *International Journal of Rock Mechanics and Mining Sciences and Geomechnics Abstracts*, Vol, 22, No. 3, pp. 121-140.

Barton, N. and De Quadros, E. F. (1997). "Joint aperture and roughness in the prediction of flow and groutability of rock masses." *International Journal of Rock Mechanics and Mining Sciences*, Vol. 34, Nos. 3-4, pp. 700-713.

Chang, Z., Zhao, Y., and Hu, Y. (2004). "Theoretic and experimental studies on seepage law of single fracture under 3D stresses." *Chinese Journal of Rock Mechanics and Engineering*, Vol. 23, No. 4, pp. 620-624. (in Chinese)

Davy, A. C., Skoczylas, F., Barnichon, J.-D., and Lebon, P. (2007). "Permeability of macro-cracked argillite under confinement: Gas and water testing." *Physics and Chemistry of the Earth*, Vol. 32, pp. 667-680.

Do Nascimento, A. F., Lunn, R. J., and Cowie, P. A. (2005). "Numerical modeling of pore-pressure diffusion in a reservoir-induced seismicity site in northeast Brazil." *Geophysical Journal International*, Vol. 160, Issue 1, pp. 249-262.

Esakia, T., Dua, S., and Mitania, Y. (1999). "Development of a shear-flow test apparatus and determination of coupled properties for a single rock joint." *International Journal of Rock Mechanics and Mining Sciences*, Vol. 36, Issue 5, pp. 641-650.

Goodman, R. E. (1976). *Methods of geological engineering in discontinuous rock*, West publishing company, New York.

Gupta, H. K. (2001). "Short-term earthquake forecasting may be feasible at Koyna, India." *Tectonophysics*, Vol. 338, Issues 3-4, pp. 353-357.

Gupta, H. K. (2002). "A review of recent studies of triggered earthquakes by artificial water reservoirs with special emphasis on earthquakes in Koyna, India." *Earth-Science Reviews*, Vol. 58, Issues 3-4, pp. 279-310.

Haji-Sotoudeh, M. (1995). *Experimental study and modeling of hydromechanical coupling in rock joints,* PhD Thesis, University of Lille 1, France.

He, Y. and Yang, L. (2004). "Testing study on variational characteristics of rockmass permeability under loading-unloading of confining pressure." *Chinese Journal of Rock Mechanics and Engineering*, Vol. 23, No. 3, pp. 415-419 (in Chinese).

Healy, J. H., Rubey, W. W., Griggs, D. T., and Raleigh, C. B. (1968). "The Denver earthquakes." *Science*, Vol. 161, No. 3848, pp. 1301-1310.

Koyama, T., Li, B., Jiang, Y., and Jing, L. (2009). "Numerical modelling of fluid flow tests in a rock fracture with a special algorithm for

contact areas." *Computers and Geotechnics*, Vol. 36, Issue 1-2, pp. 291-303.

Lee-Bell, M. and Nur, A. (2001). "Strength change due to reservoir induced pore pressure and stresses and application to Lake Oroville." *Journal of Geophysical Research*, Vol. 83, No. B9, pp. 4469-4483.

Liu, C., Chen, C., and Fu, S. (2003). "Study on seepage characteristics of a single rock fracture under shear stresses." *Chinese Journal of Rock Mechanics and Engineering*, Vol. 22, No. 10, pp. 1651-1655. (in Chinese)

Olsson, R. and Barton, N. (2001). "An improved model for hydromechanical coupling during shearing of rock joints." *International Journal of Rock Mechanics and Mining Sciences*, Vol. 38, Issue 3, pp. 317-329.

Pyrak-Nolte, L. J. and Morris, J. P. (2000). "Single fracture under normal stress: The relation between fracture specific stiffness and fluid flow." *International Journal of Rock Mechanics and Mining Sciences*, Vol. 37, Issues 1-2, pp. 245-262.

Shao, J. F., Zhou, H., and Chau, K. T. (2005). "Coupling between anisotropic damage and permeability variation in brittle rocks." *International Journal for Numerical and Analytical Methods in Geomechanics*, Vol. 29, Issue 12, pp. 1231-1247.

Snow, D. T. (1968). "Rock fracture spacings, openings, and porosities." *Journal of the Soil Mechanics and Foundations Division: Proceedings of the American Society of Civil Engineers*, Vol. 94, No. SM1, pp. 73-91.

Snow, D. T. (1969). "Anisotropic permeability of fractured media." *Water Resources Research*, Vol. 5, No. 6, pp. 1273-1289.

Tsang, Y. W. and Witherspoon, P. A. (1981) "Hydromechanical behavior of a deformable rock fracture subject to normal stress." *Journal of Geophysical Research*, Vol. 86, No. B10, pp. 9287-9298.

Tsang, Y. W. and Witherspoon, P. A. (1983). "The dependence of fracture mechanical and fluid flow properties on fracture roughness and sample size." *Journal of Geophysical Research*, Vol. 88, No. 3, pp. 2359-2366.

Witherspoon, P. A., Wang, J. S. Y., Iwai, K., and Gale, J. E. (1980). "Validity of cubic law for fluid flow in a deformable rock fracture." *Water Resources Research*, Vol. 16, No. 6, pp. 1016-1024.

Zhang, J. and Wang, J. (2006). "Coupled behavior of stress and permeability and its engineering applications." *Chinese Journal of Rock Mechanics and Engineering*, Vol. 25, No. 10, pp. 1981-1989 (in Chinese).

Zhou, C. B., Sharma, R. S., Chen, Y. F., and Rong, G. (2008). "Flow-stress coupled permeability tensor for fractured rock masses." *International Journal of Numerical and Analytical Methods in Geomechanics*, Vol. 32, No. 11, pp. 1289-1309.